Front. Med. 2021, 15(6): 913–921
https://doi.org/10.1007/s11684-021-0874-1

RESEARCH ARTICLE

^{18}F-FDG-PET glucose hypometabolism pattern in patients with epileptogenic hypothalamic hamartoma

Chao Lu[1,2,*], Kailiang Wang[1,2,*], Fei Meng[1,2], Yihe Wang[1,2], Yongzhi Shan (✉)[1,2], Penghu Wei (✉)[1,2], Guoguang Zhao (✉)[1,2,3]

[1]*Department of Neurosurgery, Xuanwu Hospital, Capital Medical University, Beijing 100053, China;* [2]*China International Neuroscience Institute (CHINA-INI), Beijing 100053, China;* [3]*Center of Epilepsy, Beijing Institute for Brain Disorder, Beijing 100069, China*

Abstract **Epileptogenic hypothalamic hamartoma is characterized by intractable gelastic seizures. A systematic analysis of the overall brain metabolic pattern in patients with hypothalamic hamartoma (HH) could facilitate the understanding of the epileptic brain network and the associated brain damage effects of HH. In this study, we retrospectively evaluated 27 patients with epileptogenic HH (8 female patients; age, 2–33 years) by using ^{18}F-fluorodeoxyglucose-positron emission tomography. The correlations among tomography result, seizure type, sex, and structural magnetic resonance imaging were assessed. Whole metabolic patterns and voxel-based morphometry findings were assessed by group analysis with healthy controls. Assessment of the whole metabolic pattern in patients with HH revealed several regional metabolic reductions in the cerebrum and an overall metabolic reduction in the cerebellum. In addition, areas showing hypometabolism in the neocortex were more widely distributed ipsilaterally than contralaterally to the HH. Reductions in glucose metabolism and gray matter volume in the neocortex were predominant ipsilateral to the HH. In conclusion, the glucose hypometabolism pattern in patients with epileptogenic HH involved the neocortex, subcortical regions, and cerebellum. The characteristics of glucose hypometabolism differed across seizure type and sex. Reductions in glucose metabolism and structural changes may be based on different mechanisms, but both are likely to occur ipsilateral to the HH in the neocortex. We hypothesized that the dentato-rubro-thalamic tract and cerebro-ponto-cerebellar tract, which are responsible for intercommunication between the cerebral cortex, subcortical regions, and cerebellar regions, may be involved in a pathway related to seizure propagation, particularly gelastic seizures, in patients with HH.**

Keywords hypothalamic hamartoma; gelastic seizure; fluorodeoxyglucose-positron emission tomography; voxel-based morphometry

Introduction

Hypothalamic hamartoma (HH) is a rare, congenital, developmental malformation arising from the floor of the third ventricle, tuber cinereum, or mammillary bodies. Epileptogenic HH is characterized by intractable gelastic seizures (GS), which are occasionally accompanied by precocious puberty, progressive cognitive impairment, and behavioral disorders [1]. GS has been recognized as a specific form of epileptic seizure since 1873. Breningstall *et al.* [2] described HH and paroxysmal laughter in detail and proposed the association among GS, HH, and precocious puberty syndrome. Patients with HH can develop various types of seizures over time, including dacrystic seizures, focal impaired awareness seizures (FIAS), typical absence seizures (TBS), and focal to bilateral tonic-clonic seizures (FBTCS).

Previous studies reported the critical role of HH during seizure onset [3–5]. However, a lack of comprehensive understanding of the cortex microstructural variations and glucose metabolism patterns related to HH persists. An increasing number of imaging studies have focused on structural changes in gray matter (GM) and white matter (WM) in patients with epilepsy [6–8]. Voxel-based morphometry (VBM) analysis is widely used to detect

Received March 8, 2021; accepted May 29, 2021

Correspondence: Yongzhi Shan, shanyongzhi@xwhosp.org;
Penghu Wei, weipenghu@xwhosp.org;
Guoguang Zhao, ggzhao@vip.sina.com

*The two authors contributed equally to this article.

changes in GM volume (GMV). Furthermore, ^{18}F-fluorodeoxyglucose-positron emission tomography (^{18}F-FDG-PET) can reveal areas of interictal brain hypometabolism associated with epileptic activity and epileptogenic lesions. This tool is applied for presurgical evaluation of the epileptogenic zone (EZ) [9,10]. A systematic analysis of overall brain metabolic patterns in patients with HH could enhance our understanding of the epileptic brain network and associated brain damage effects of HH. Results provide a reference for presurgical evaluations and clinical treatment plans.

This study aimed to detect abnormal brain metabolic regions and compare GMV changes in patients with HH. We described structural GMV differences and ^{18}F-FDG-PET glucose hypometabolism patterns in a series of 27 patients with epileptogenic HH.

Materials and methods

Participants

This retrospective study included patients with HH who had epileptic symptoms and who met the criteria for drug-resistant epilepsy as defined by the International League Against Epilepsy.

Fifty-two patients with epileptogenic HH were considered as candidates for surgical treatment between July 2015 and August 2020 in the Department of Neurosurgery, Xuanwu Hospital, Capital Medical University. Comprehensive non-invasive presurgical evaluations including semiology, video-electroencephalography (EEG), and structural magnetic resonance imaging (MRI) were performed for all subjects. HH was diagnosed based on the MRI findings of a GM mass posterior to the pituitary stalk, between the optic chiasm and the midbrain, which is typically isointense to normal GM on T1W1 imaging and isointense to slightly hyperintense on T2W1/fluid-attenuated inversion-recovery imaging. Further neuroimaging investigation was performed using FDG-PET scans to meet the needs of clinical presurgical evaluation for some patients with multiple seizure symptoms including, but not limited to, GS or severe complications. Patients with (1) non-epileptogenic HH, (2) without FDG-PET examination data, and (3) with a history of neocortectomy were excluded from this study. Twenty-eight patients with drug-resistant seizure underwent FDG-PET, and one of the patients was excluded due to a history of left temporal lobe neocortectomy. Twenty-seven patients with HH were finally selected for the analysis. Patients with HH can develop one or multiple types of seizures. GS was the most common type. In this study, 26/27 patients had GS, 15 patients had FBTCS (1 patient with FBTCS alone and 14 patients with coexistent GS), and 12 patients had FIAS (4/12) or TBS (8/12). Considering that patients with FBTCS formed the largest group, except for patients with GS, and FBTCS was identified as a special classification, we placed patients into the FBTCS and non-FBTCS groups according to seizure type for further analysis. In addition, patients were stratified into the male and female groups according to sex. The FDG-PET images of 25 healthy controls and 3D T1-weighted MRI scans of 31 healthy controls were used for statistical analysis. Informed consent was obtained from all patients.

MRI data acquisition, pre-processing, and analysis

All patients underwent MRI magnetization-prepared rapid gradient-echo sequence (MPRAGE) (1 mm, gadolinium contrast after normal scan, Siemens 3T). An experienced rater classified the location of the HH as left-side predominant, right-side predominant, or non-lateralized. The non-lateralized group was further classified as left-side or right-side predominant based on the laterality of the epileptic discharge on scalp electroencephalogram (EEG).

MRI data were pre-processed voxel-by-voxel by using Computational Anatomy Toolbox (CAT12) in Statistical Parametric Mapping version 12 (SPM12) on MATLAB 2015a (MathWorks, Inc., Natick, MA, USA), as described previously [11]. The MRI images were co-registered with the Montreal Neurological Institute (MNI)-ICBM Average Brain 152 atlas for spatial normalization. The co-registered MRI images were segmented into GMV, WM volume, and cerebrospinal fluid (CSF) images. The modulated and spatially normalized segments from each subject were spatially smoothed with an 8 mm full-width at half-maximum (FWHM) Gaussian kernel. For further data analysis, the MRI images of the HH classified as having a left-side dominant location were left-right flipped to ensure a homogeneous group such that all patients had an ipsilateral seizure propagation path given that the consistency of epileptic discharge and hypometabolism in HH was proven in previous studies.

A VBM analysis was performed to assess GMV differences between patients with HH and healthy controls, with age, sex, and total intracranial volume (TIV) as covariates.

^{18}F-FDG-PET data acquisition, pre-processing, and analysis

PET images were acquired using a United Imaging PET scanner (United Imaging, Shanghai, China). Patients were instructed to fast for at least 6 h and rest in a semi-dark room with eyes closed and ears unplugged for 30 min after an intravenous injection of 3.7 MBq/kg ^{18}F-FDG. PET images were acquired 30–40 min after the injection, providing 2.4 mm slices, with an isotropic spatial resolution of 5 mm. We expected no seizure to occur within 12 h prior to the examination. The position of the

patients' heads was stabilized during the scan to ensure optimum image quality. The PET data were analyzed using SPM12 in MATLAB 2015a. For the initial analysis, SPM12 was used to co-register the PET image of each participant to the individual T1W1 MRI space. The co-registered MR/PET images were then co-registered with an SPM T1W1 MRI template reference and smoothed with an 8 mm FWHM Gaussian kernel to optimize the PET image analysis. The FDG data sets were normalized into a common MNI atlas by using the following three-step procedure: (1) the processed PET images were spatially normalized to the MNI-ICBM Average Brain 152 atlas; (2) the PET image values were normalized to the average whole brain uptake and proportionally scaled to a mean value of 50 to reduce individual variation; and (3) the PET images of patients with left-side dominant HH were then left-right flipped for further analysis.

FDG-PET data were analyzed to determine metabolic differences between patients with HH and healthy controls and between the FBTCS group and non-FBTCS group, with age and sex as covariates. An analysis of metabolic differences was also carried out between the female and male groups, with age as the covariate.

Statistical analysis

Demographic data were analyzed using SPSS (version 20.0; SPSS Inc., Chicago, IL, USA). Between-group comparisons of age were performed using Mann–Whitney U tests, and group differences based on sex were analyzed using Chi-square tests, with P value < 0.01 as the pre-specified threshold.

For VBM and ^{18}F-FDG-PET data analysis, neuroimaging data were entered into the general linear modeling (GLM) analysis using SPM12. The data were compared between patients with HH and healthy controls, with age and sex as covariates, and used to map the specified epileptic hypometabolic pattern in the patients. According to seizure type and sex, patients with HH were divided into FBTCS and non-FBTCS groups as well as male and female groups, respectively; these groups were compared by two-sample t-test. $P < 0.01$ was considered significant, and the cluster extent was set to $k > 50$. When multiple statistical tests were performed, false discovery rate (FDR) or Bonferroni multiple comparison methods were used to reduce false positives.

Results

Demographic and clinical results

Mann–Whitney U tests demonstrated that patients with HH were significantly younger than healthy controls (both MRI and PET data groups) ($P < 0.01$). Chi-square tests showed significantly fewer female patients in the patient group than in the MRI healthy control group and PET healthy control group ($P < 0.01$). Table 1 shows the detailed demographic information of patients with HH and healthy controls.

Table 1 Demographic data

	HH patients	Healthy controls (PET group)	Healthy controls (VBM group)
Total number	27	25	31
Age (year (mean±SD))	3–33 (12±11)	31–68 (44±16)	18–29 (24±3)
Sex (*n*)			
Male	19	10	10
Female	8	15	21
Seizure type (*n*)			
GS	26	–	–
FBTCS	15	–	–
FIAS	4	–	–
TBS	8	–	–

According to the classification of the laterality of the HH mass on MRI, 10 of the 27 patients were classified as having left-side predominant HH; 14 with right-side predominant HH; and 3 with non-lateralized HH. The non-lateralized group was further classified based on left- or right-side predominance according to the laterality of epileptic discharge on scalp EEG. One patient was classified as having left-side predominant HH, and two patients had right-side predominant HH. The images of 11 patients with left-side predominant HHs were left-right flipped for further analysis.

Metabolic changes

^{18}F-FDG-PET whole metabolic pattern difference

The glucose metabolic uptake pattern of patients with HH showed several regional metabolic reductions in the cerebrum and an overall reduction in the cerebellum. Analysis of glucose metabolic uptake revealed select subgroup differences after statistical adjustment for the impact of covariates in the analysis and FDR correction. Patients with HH displayed significantly hypometabolic areas compared with healthy controls in the following identified clusters: (1) the bilateral post cingulum, (2) the frontal lobe ipsilateral to HH, (3) the bilateral occipital lobes, (4) the bilateral temporal lobes, (5) the bilateral hippocampus, (6) the bilateral parahippocampus, (7) the bilateral amygdala, (8) the bilateral thalamus, red nucleus, and globes pallidus, (9) the brainstem and bilateral midbrain, and (10) the bilateral cerebellum (Fig. 1). Table 2 lists the MNI coordinates and T values of the

identified regions. No significantly hypermetabolic areas were found in the patients compared with the healthy controls. The cortex was involved bilaterally, except for the frontal lobe. In clusters (1), (3), (4), (5), (6), (7), and (8), the extent of hypometabolic areas was greater ipsilateral to the HH rather than contralateral to the HH; by contrast, the involved areas of clusters (9) and (10) were symmetrically distributed on the left and right.

Metabolic difference between FBTCS and non-FBTCS groups

Compared with the non-FBTCS group, HH patients with FBTCS demonstrated a significant reduction in glucose metabolic uptake on both sides of the precentral gyrus and insular lobe ipsilateral to HH. A significant increment in glucose metabolic uptake was found in the area of the cerebellum ipsilateral to the HH, indicating that the non-FBTCS group had significant hypometabolism compared with the FBTCS group (Fig. 2A).

Metabolic difference between the sexes

Metabolic differences between female and male patients with HH were assessed. A difference in glucose metabolism was found in both hemispheres. The female patients showed significantly hypometabolic regions compared with the male patients in the following clusters: (1) bilateral frontal lobes, (2) temporal lobe ipsilateral to HH, (3) cingulum contralateral to HH, and (4) bilateral parietal lobes. In the regions of bilateral superior parietal lobes and precentral gyrus, male HH patients showed a significant reduction in glucose metabolic uptake compared with female patients (Fig. 2B).

Comparison of PET and VBM

The total mean GMV did not differ between HH patients and healthy controls ($P > 0.01$). However, VBM analysis demonstrated a significant difference in the cortical structure between patients with HH and healthy controls. The healthy control group showed significantly greater regional GMV than the patient group mainly in the hemisphere ipsilateral to the HH. By contrast, the patient group displayed significantly greater regional GMV in the hemisphere contralateral to the HH, especially in the frontal and temporal lobes. The GMV in the subcortical structures, including the bilateral caudate nucleus and thalamus contralateral to the HH, was significantly decreased. However, the GMV of the cerebellum in patients with HH was significantly increased (Fig. 3). We further compared the ^{18}F-FDG-PET metabolic patterns of

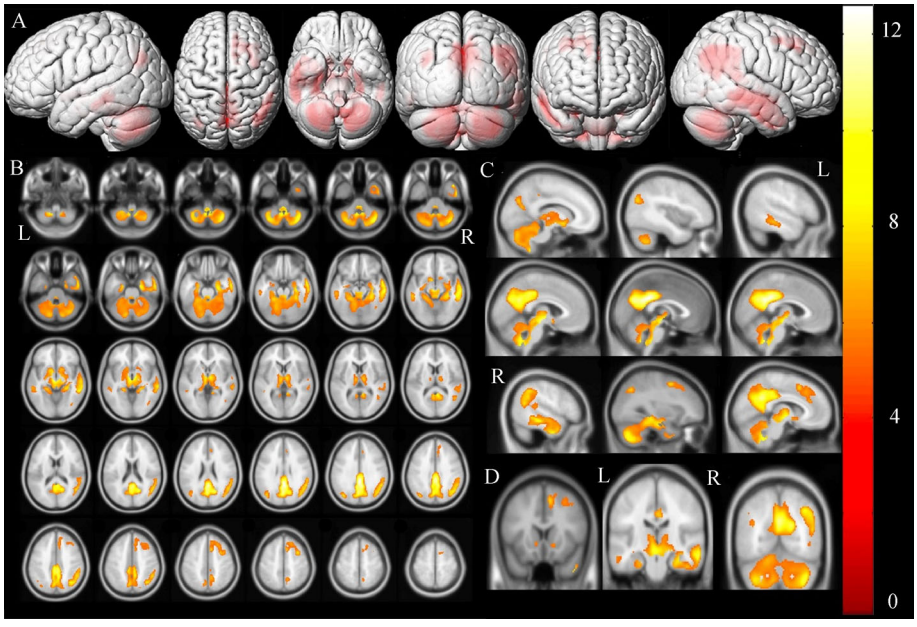

Fig. 1 Differences in whole brain metabolic patterns between patients with hypothalamic hamartoma (HH) and healthy controls ($P < 0.01$; two-sample *t*-test). The red-yellow color indicates a decrease in the metabolism. (A) three-dimensional (3-D) surface view of metabolic maps. Hypometabolism is mainly distributed in the right hemisphere ipsilateral to the HH, involving the frontal lobe, temporal lobe, parietal lobe, and occipital lobe. Meanwhile, hypometabolism is seen in small parts of the contralateral temporal and parietal lobes. Moreover, hypometabolism is seen in the bilateral cerebellum. (B) Axial view maps are more detailed than the 3-D surface view maps. Apart from the surface, bilateral regions, such as the thalamus, red nucleus, and globus pallidus, are also involved in the hypometabolic pattern. (C) Sagittal view maps show distinct involvement of the bilateral cingulum, an essential part of the default mode network, the thalamus, and the cerebellum, which are connected by the dentato-rubro-thalamic tract. (D) Coronal view maps. L, left; R, right.

Table 2 Brain regions showing significant metabolic differences between patients and healthy controls

Cluster	Region	MNI coordinate (mm)			*T* value
		X	*Y*	*Z*	
(1)	Cingulum_Post_L	2	–42	30	12.54
	Cingulum_Post_R	4.39	–40	30	11.79
(2)	Frontal_Mid_R	32	6	50	7.82
	Supp_Motor_Area_R	8	15.65	48	7.19
	Precentral_R	34.64	1.99	50	6.5
(3)	Angular_R	36.59	–66.28	40	8.3
	Angular_L	–39.52	–70.18	30	6.87
	Occipital_Mid_L	–38	–74	32	7.82
(4)	Temporal_Mid_L	–54	–32	–12	6.97
	Temporal_Mid_R	55.13	–32	–14	8.14
(5)	Hippocampus_R	28.78	–9.17	–24	7.6
	Hippocampus_L	–20	–6	–26	7.36
(6)	ParaHippocampal_R	24.88	–10.69	–28	8.62
	ParaHippocampal_L	–21.95	–10	–30	6.78
(7)	Amygdala_L	–22.93	–3.86	–26	6.75
	Amygdala_R	27.81	–2.88	–24	6.47
(8)	Thalamus_L	–3.42	–12.84	–2	8.67
	Thalamus_R	8.29	–8.73	–2	8.71
(9)	Mid_brain _L	–2.44	–20.44	–6	8.6
	Mid_brain _R	7.32	–17.51	–8	7.92
	Brianstem	–0.49	–32.14	–16	6.88
(10)	Cerebellum_L	–33.66	–60	–46.82	7.79
	Cerebellum_R	36.59	–64	–45.84	9.45

L, left; R, right.

HH patients with the results of VBM analysis to determine the relationship between metabolism and structural abnormalities. The side with predominant reductions in glucose metabolism and GMV was ipsilateral to the HH, covering the frontal lobe, temporal lobe, parietal lobe, and occipital lobe. These regions were not completely consistent because the range of GMV decrease was greater than the hypometabolism in the neocortex, as shown in the PET results. In the subcortical regions and cerebellum, PET revealed significant reductions in glucose metabolism, but VBM analysis revealed a decrease in GMV in the bilateral caudate nucleus and contralateral thalamus and a GMV increase in the bilateral cerebellum, which was unrelated to the topography of metabolic changes.

Discussion

This study revealed significant differences in whole metabolic patterns on ^{18}F-FDG-PET and regional GMV between patients with HH and healthy controls. Differences in glucose metabolism were analyzed according to seizure type and sex. The hypometabolic regions corresponded to regions with decreased GMV to a certain extent in patients with HH. These findings have rarely been reported in patients with HH and may reveal novel insights into the mechanism of epileptogenic HH.

Previous studies using ^{18}F-FDG-PET demonstrated that hypometabolism in the brain is usually associated with the origin and propagation of epilepsy [12,13]. The critical

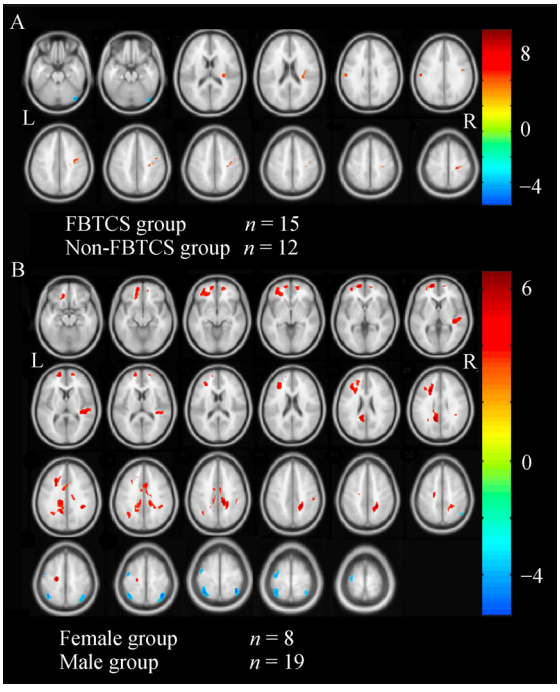

Fig. 2 Metabolic differences according to seizure type and sex ($P < 0.01$). The red-yellow color indicates the decrease in metabolism, and the blue-green color indicates the increase in metabolism. (A) Metabolic difference between the different seizure types. HH patients with focal to bilateral tonic–clonic seizure (FBTCS) show significant hypometabolism on both sides of the precentral gyrus and insular lobe ipsilateral to the HH and hypermetabolism in the right cerebellum compared with the non-FBTCS patients. (B) Metabolic difference between sexes. Female patients show significant hypometabolism in the bilateral frontal lobes and parietal lobes, right temporal lobe, and left cingulate gyrus and hypermetabolism in the bilateral superior parietal lobes and left precentral gyrus compared with the male patients. L, left; R, right.

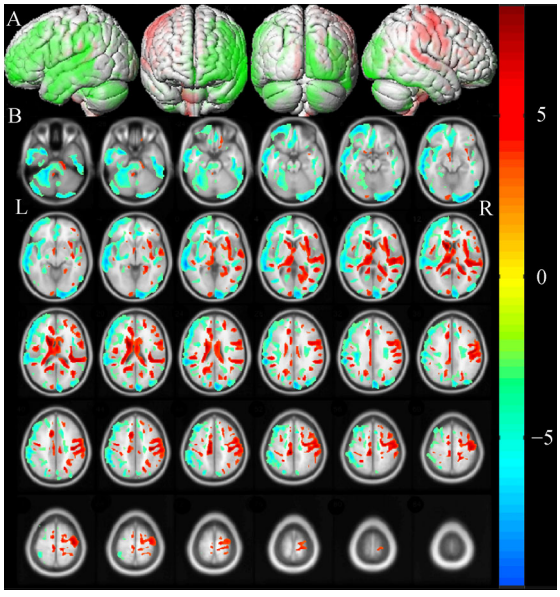

Fig. 3 Voxel-based morphometry (VBM) results of HH patients and healthy controls ($P < 0.01$, two-sample *t*-test). Gray matter volume (GMV) decrease is shown in blue-green, and GMV increase is shown in red-yellow. (A) 3-D surface view of VBM results. HH patients show significant GMV decrease in the hemisphere ipsilateral to HH and GMV increase in the hemisphere contralateral to HH, especially in the regions of the frontal and temporal lobes. Overall, the GMV in the cerebellum increases. (B) Axial view maps showing more details than 3-D surface view maps. L, left; R, right.

role of HH during seizure onset was reported [3,14]. Two distinct populations of small clustered GABA-expressing neurons and large pyramidal-like neurons have been found in HH, and the small neurons are believed to be the "pacemaker" of the intrinsic epileptogenicity of HH [15]. A recent stereo-EEG study confirmed that interictal biomarkers, similar to high-frequency oscillation, can be detected within HH, and authors concluded that different onset patterns of preictal discharge, ictal fast activity, and simultaneous direct shift are related to HH [16]. Neuroimaging studies on HH could help analyze seizure propagation and better understand the epileptic network. Ryvlin *et al.* described the first series of five patients to investigate FDG-PET in epileptic HHs [17]. They hypothesized that the hypometabolic lobar within the HH, ipsilateral to the predominant EEG abnormalities and side of the HH, tended to match that of the cortical network suspected to be predominantly involved in non-GS. Our previous PET case series revealed three patterns of hypometabolic characteristics of the extra-hypothalamic cortex in HH [18]. In the present study, we analyzed the ^{18}F-FDG-PET whole metabolic pattern difference identified in 10 clusters between patients with HH and healthy controls.

The default mode network (DMN), which demonstrates increased brain activity at rest, is related to several types of epilepsy [19]. The network is also related to the impairment of attention and cognitive dysfunction [19–21]. In the present study, the regions of the DMN, especially the bilateral post cingulate cortex (PCC), were found to be involved in the hypometabolism pattern. Another FDG-PET study on cognitive impairment in patients with HH revealed that patients with cognitive impairment showed a reduction in glucose metabolism in regions of the PCC, the highly efficient network nodes in the DMN. Frontal and temporal lobes are believed to be involved in HH-related seizure propagation based on PET neuroimaging [17] and stereo-EEG studies [3]. In the present work, we observed that the hypometabolic areas of the frontal lobe are ipsilateral to the HH, mainly including the middle frontal gyrus, supplemental motor area, precentral gyrus, and bilateral temporal lobes. Moreover, the limbic system, comprising the amygdala, hippocampus, parahippocampal gyrus, dentate gyrus, cingulate

gyrus, and mammillary bodies, was included in the metabolic pattern. As a crucial node of HH-related seizure propagation, the mammillary body could propagate epileptic discharge through the fibers in the Papez circuit to other limbic system regions. The metabolic differences in the brainstem and bilateral cerebellum significantly differ from the patterns observed in other types of epilepsy, such as temporal lobe epilepsy [22,23]. An early single-photon emission tomography (SPECT)-based case study showed hypoperfusion in the bilateral frontoparietal region and in both cerebellar hemispheres; this abnormality may be due to the spread of the cortical epileptogenic focus and complex intercommunication between the frontal cortex and cerebellar hemispheres [24]. Activation in subcortical structures, with early time-shift models, and the cerebellum, with later time-shift models, was observed in the analysis of an EEG-fMRI group [25]. Lesion studies revealed that the cerebellar structures automatically adjust the execution of laughter or crying to the cognitive and situational context of a potential stimulus [26–28]. We hypothesized that the dentato-rubro-thalamic tract (DRTT) and the cerebro-ponto-cerebellar tract intercommunicating between the cerebral cortex, subcortical regions, and cerebellar regions are potential pathways for HH-related seizure propagation, especially that of GS, considering the simultaneous hypometabolism observed in the bilateral thalamus, red nucleus, and cerebellum. If the roles of these circuits could be corroborated by future studies, the essential nodes may serve as the target of epilepsy neuromodulation, such as by non-invasive transcranial direct current stimulation or repetitive transcranial magnetic stimulation.

Reduced glucose metabolism in the bilateral precentral gyrus and insular lobe ipsilateral to the HH was observed in HH patients with FBTCS compared with that in HH patients without FBTCS. GS is a characteristic seizure type of epileptogenic HH. Other seizure types may appear during the evolution of the condition, probably resulting from secondary epileptogenic mechanisms [29]. This finding supports the hypothesis that different parts of the brain involved in the seizure network lead to different patterns of HH onset. Differences in brain development and maturation could be influenced by sex-related effects on epilepsy susceptibility [30]. Epidemiological investigations suggested that women are more susceptible to HH. With respect to the PET results, we found significant differences in multiple lobes according to the sex of the subjects, especially in the frontal lobe contralateral to HH. We could not confirm the significance of these regions due to lack of neuropsychological assessment results. However, our results suggest that female patients are more susceptible to HH progression than male patients.

Few studies focused on the whole brain structure in HH, which is a lesion-based epilepsy. To verify the relationship between hypometabolism and structural changes, we performed VBM to detect GMV difference. In this study, we found that the regions of hypometabolism and structural changes were not completely consistent. However, their lateralization was essentially the same, implying that the hypometabolic zone and the regions with decreased GMV in the neocortex were mainly concentrated to a location ipsilateral to the HH. Although GMV decrease and glucose metabolic reduction are based on different underlying mechanisms, both were ipsilateral to the HH. In contrast to the metabolic results, the GMV significantly increased in the neocortex, contralateral to the HH and bilateral cerebellum, which is usually interpreted as a compensatory mechanism. Metabolic and macroscopic changes in brain maturation and functional connections can result from hamartomas. An extensive overlap existed between the hypometabolism regions and areas with decreased GMV. The overlapping regions with metabolic and structural alterations essentially involved the superior frontal gyrus, temporal lobe ipsilateral to HH and bilateral PCC, and caudate nucleus. This broad similarity in the altered and preserved cerebral regions points to a causal relationship between atrophy and hypometabolism. For instance, progressive neuronal loss may induce local hypometabolism; conversely, any prolonged metabolic disruption may consequently lead to neuronal loss [31]. Moreover, certain regional variations in the differences between structural changes and metabolism abnormalities were found. The most distinct difference was the significant compensation in the GMV structure on the contralateral side of HH, whereas metabolism revealed no such significant change. Thus, the relationship between these changes is not uniform across the brain, indicating that the compensation of brain structure is an independent phenomenon of the disease and not solely a result of metabolic variation. A previous study detected structural differences in GM and WM densities between children with HH with only gelastic seizure and those with multiple seizure types [32]. A difference in WM density was found in the temporal lobe and cerebellum, confirming structural differences outside the hamartoma mass in HH. In the present study, we analyzed the structural difference in HH by using a group of normal controls. Finding age-matched healthy controls is difficult because of the younger age of patients with HH. Thus, the VBM analysis results may have been biased despite using age, gender, and TIV as covariates.

Limitations

This study has a number of limitations. The study sample mainly included HH patients with multiple seizure types; we lacked PET data for patients with HH with GS alone to analyze the GS network. The paucity of the results from neuropsychological assessments prevented further analysis

of the significance of the involved areas given that HH is accompanied by progressive cognitive impairment and behavioral disorders. The age mismatch between the two groups could have caused bias. Further studies on seizure networks with cognitive and age-matched group analysis through PET or stereo-EEG may be necessary.

Conclusions

In this study, we identified 10 clusters, involving the neocortex, subcortical regions, and cerebellum, that showed glucose hypometabolism patterns on ^{18}F-FDG-PET in patients with epileptogenic HH. The range of glucose hypometabolism was more extensive in the female participants than in male participants. The regions displaying hypometabolism and decreased GMV in the neocortex were mainly concentrated ipsilateral to HH. We hypothesized that the DRTT and cerebro-ponto-cerebellar tract intercommunicating between the cerebral cortex, subcortical regions, and the cerebellar regions could be potential pathways for the propagation of seizures, especially GS, in patients with HH.

Acknowledgements

This work was supported by the National Natural Science Foundation of China (Nos. 81801288, 81871009, and 82030037)

Compliance with ethics guidelines

Chao Lu, Kailiang Wang, Fei Meng, Yihe Wang, Yongzhi Shan, Penghu Wei, and Guoguang Zhao declare that they have no conflicts of interest. All procedures were conducted in accordance with the ethical standards of the responsible committee on human experimentation (institutional and national) and with the *Helsinki Declaration* of 1975, as revised in 2000 (5). Informed consent was obtained from all patients for inclusion in the study.

References

1. Wagner K, Schulze-Bonhage A, Urbach H, Trippel M, Spehl TS, Buschmann F, Metternich B, Ofer I, Meyer PT, Frings L. Reduced glucose metabolism in neocortical network nodes remote from hypothalamic hamartomas reflects cognitive impairment. Epilepsia 2017; 58(Suppl 2): 41–49
2. Breningstall GN. Gelastic seizures, precocious puberty, and hypothalamic hamartoma. Neurology 1985; 35(8): 1180–1183
3. Wang D, Shan Y, Bartolomei F, Kahane P, An Y, Li M, Zhang H, Fan X, Ou S, Yang Y, Wei P, Lu C, Wang Y, Du J, Ren L, Wang Y, Zhao G. Electrophysiological properties and seizure networks in hypothalamic hamartoma. Ann Clin Transl Neurol 2020; 7(5): 653–666
4. Kahane P, Ryvlin P, Hoffmann D, Minotti L, Benabid AL. From hypothalamic hamartoma to cortex: what can be learnt from depth recordings and stimulation? Epileptic Disord 2003; 5(4): 205–217
5. Wu J, Xu L, Kim DY, Rho JM, St John PA, Lue LF, Coons S, Ellsworth K, Nowak L, Johnson E, Rekate H, Kerrigan JF. Electrophysiological properties of human hypothalamic hamartomas. Ann Neurol 2005; 58(3): 371–382
6. Mueller SG, Laxer KD, Cashdollar N, Buckley S, Paul C, Weiner MW. Voxel-based optimized morphometry (VBM) of gray and white matter in temporal lobe epilepsy (TLE) with and without mesial temporal sclerosis. Epilepsia 2006; 47(5): 900–907
7. Barron DS, Fox PM, Laird AR, Robinson JL, Fox PT. Thalamic medial dorsal nucleus atrophy in medial temporal lobe epilepsy: a VBM meta-analysis. Neuroimage Clin 2013; 2: 25–32
8. Labate A, Cerasa A, Gambardella A, Aguglia U, Quattrone A. Hippocampal and thalamic atrophy in mild temporal lobe epilepsy: a VBM study. Neurology 2008; 71(14): 1094–1101
9. Ponisio MR, Zempel JM, Day BK, Eisenman LN, Miller-Thomas MM, Smyth MD, Hogan RE. The role of SPECT and PET in epilepsy. AJR Am J Roentgenol 2021; 216(3): 759–768
10. Shang K, Wang J, Fan X, Cui B, Ma J, Yang H, Zhou Y, Zhao G, Lu J. Clinical value of hybrid TOF-PET/MR imaging-based multiparametric imaging in localizing seizure focus in patients with MRI-negative temporal lobe epilepsy. AJNR Am J Neuroradiol 2018; 39(10): 1791–1798
11. Vickery S, Hopkins WD, Sherwood CC, Schapiro SJ, Latzman RD, Caspers S, Gaser C, Eickhoff SB, Dahnke R, Hoffstaedter F. Chimpanzee brain morphometry utilizing standardized MRI preprocessing and macroanatomical annotations. eLife 2020; 9: e60136
12. Lamarche F, Job AS, Deman P, Bhattacharjee M, Hoffmann D, Gallazzini-Crépin C, Bouvard S, Minotti L, Kahane P, David O. Correlation of FDG-PET hypometabolism and SEEG epileptogenicity mapping in patients with drug-resistant focal epilepsy. Epilepsia 2016; 57(12): 2045–2055
13. Lagarde S, Boucekine M, McGonigal A, Carron R, Scavarda D, Trebuchon A, Milh M, Boyer L, Bartolomei F, Guedj E. Relationship between PET metabolism and SEEG epileptogenicity in focal lesional epilepsy. 2020; 47: 3130–3142
14. Wei PH, An Y, Fan XT, Wang YH, Yang YF, Ren LK, Shan YZ, Zhao GG. Stereoelectroencephalography-guided radiofrequency thermocoagulation for hypothalamic hamartomas: preliminary evidence. World Neurosurg 2018; 114: e1073–e1078
15. Fenoglio KA, Wu J, Kim DY, Simeone TA, Coons SW, Rekate H, Rho JM, Kerrigan JF. Hypothalamic hamartoma: basic mechanisms of intrinsic epileptogenesis. Semin Pediatr Neurol 2007; 14(2): 51–59
16. Wang D, Shan Y, Bartolomei F, Kahane P, An Y, Li M, Zhang H, Fan X, Ou S, Yang Y, Wei P, Lu C, Wang Y, Du J, Ren L, Wang Y, Zhao G. Electrophysiological properties and seizure networks in hypothalamic hamartoma. Ann Clin Transl Neurol 2020; 7(5): 653–666
17. Ryvlin P, Ravier C, Bouvard S, Mauguire F, Le Bars D, Arzimanoglou A, Petit J, Kahane P. Positron emission tomography in epileptogenic hypothalamic hamartomas. Epileptic Disord 2003; 5(4): 219–227
18. Yang YF, Wei PH, Meng F, An Y, Fan XT, Wang YH, Wang D, Ren LK, Shan YZ, Zhao GG. Glucose metabolism characteristics of extra-hypothalamic cortex in patients with hypothalamic hamarto-

mas (HH) undergoing epilepsy evaluation: a retrospective study of 16 cases. Front Neurol 2021; 11: 587622

19. McCormick C, Protzner AB, Barnett AJ, Cohn M, Valiante TA, McAndrews MP. Linking DMN connectivity to episodic memory capacity: what can we learn from patients with medial temporal lobe damage? Neuroimage Clin 2014; 5: 188–196
20. Hu CY, Gao X, Long L, Long X, Liu C, Chen Y, Xie Y, Liu C, Xiao B, Hu ZY. Altered DMN functional connectivity and regional homogeneity in partial epilepsy patients: a seventy cases study. Oncotarget 2017; 8(46): 81475–81484
21. Mohan A, Roberto AJ, Mohan A, Lorenzo A, Jones K, Carney MJ, Liogier-Weyback L, Hwang S, Lapidus KAB. The significance of the default mode network (DMN) in neurological and neuropsychiatric disorders: a review. Yale J Biol Med 2016; 89(1): 49–57
22. Wang KL, Hu W, Liu TH, Zhao XB, Han CL, Xia XT, Zhang JG, Wang F, Meng FG. Metabolic covariance networks combining graph theory measuring aberrant topological patterns in mesial temporal lobe epilepsy. CNS Neurosci Ther 2019; 25(3): 396–408
23. Chassoux F, Artiges E, Semah F, Desarnaud S, Laurent A, Landré E, Gervais P, Devaux B, Helal OB. Determinants of brain metabolism changes in mesial temporal lobe epilepsy. Epilepsia 2016; 57(6): 907–919
24. Iannetti P, Spalice A, Raucci U, Atzei G, Cipriani C. Gelastic epilepsy: video-EEG, MRI and SPECT characteristics. Brain Dev 1997; 19(6): 418–421
25. Usami K, Matsumoto R, Sawamoto N, Murakami H, Inouchi M, Fumuro T, Shimotake A, Kato T, Mima T, Shirozu H, Masuda H, Fukuyama H, Takahashi R, Kameyama S, Ikeda A. Epileptic network of hypothalamic hamartoma: an EEG-fMRI study. Epilepsy Res 2016; 125: 1–9
26. Parvizi J, Anderson SW, Martin CO, Damasio H, Damasio AR. Pathological laughter and crying: a link to the cerebellum. Brain 2001; 124(9): 1708–1719
27. Elyas AE, Bulters DO, Sparrow OC. Pathological laughter and crying in patients with pontine lesions. J Neurosurg Pediatr 2011; 8(6): 544–547
28. Zhang L, Cao B, Wei QQ, Ou R, Zhao B, Yang J, Wu Y, Shang H. Pathological laughter and crying in multiple system atrophy with different subtypes: frequency and related factors. J Affect Disord 2021; 283: 60–65
29. Striano S, Striano P. Clinical features and evolution of the gelastic seizures-hypothalamic hamartoma syndrome. Epilepsia 2017; 58(Suppl 2): 12–15
30. Savic I, Engel J Jr. Structural and functional correlates of epileptogenesis—does gender matter? Neurobiol Dis 2014; 70: 69–73
31. Chételat G, Landeau B, Eustache F, Mézenge F, Viader F, de la Sayette V, Desgranges B, Baron JC. Using voxel-based morphometry to map the structural changes associated with rapid conversion in MCI: a longitudinal MRI study. Neuroimage 2005; 27(4): 934–946
32. Losey TE, Beeman SC, Ng YT, Kerrigan JF, Baxter LC. White matter density is increased in patients with hypothalamic hamartoma and multiple seizure types. Epilepsy Res 2011; 93(2–3): 212–215